JOURNAL OF RAMAN SPECTROSCOPY
J. Raman Spectrosc. 2007; **38**: 802–818
Published online 2 March 2007 in Wiley InterScience
(www.interscience.wiley.com) DOI: 10.1002/jrs.1695

JRS

Raman and surface-enhanced Raman spectra of flavone and several hydroxy derivatives

Tatyana Teslova,[1†] Charlie Corredor,[1†] Richard Livingstone,[1] Tudor Spataru,[1] Ronald L. Birke,[1] John R. Lombardi,[1*] M. V. Cañamares[2] and Marco Leona[2]

[1] Department of Chemistry and Center for Study of Structures and Interfaces (CASI), The City College of New York, New York, N.Y. 10031
[2] The Metropolitan Museum of Art, 1000 Fifth Avenue, New York, N.Y. 10028

Received 19 September 2006; Accepted 5 December 2006

The Raman and surface-enhanced Raman spectra (SERS) of flavone and three of its hydroxy derivatives, 3-hydroxyflavone (3-HF) and 5-hydroxyflavone (5-HF) and quercetin (3,5,7,3′,4′ pentahydroxyflavone) have been obtained. The normal Raman (NR) spectra were taken in the powder form. The SERS spectra were obtained both on Ag colloids and Ag electrode substrates. Assignments of the spectrally observed normal modes were aided by density functional theory (DFT) calculations using the B3LYP functional and the 6-31+G* basis, a split valence polarized basis set with diffuse functions. Excellent fits were obtained for the observed spectra with little or no scaling. The most intense lines of the NR spectra are those in the C═O stretching region (near 1600 cm^{-1}). These lines are often weakened by proximity to the surface, while other lines at lower wavenumbers, due to in-plane ring stretches, tend to be strongly enhanced. The SERS spectrum of flavone is weak both on the colloid and on the electrode, indicating weak attachment to the surface. In contrast, the SERS spectra of the hydroxy derivatives of flavone are intense, indicating the assistance of OH groups in attachment to the surface. The spectra of the various species are compared, and a case study of application to detection of a textile dye (Persian berries), which contains quercetin, is presented. Copyright © 2007 John Wiley & Sons, Ltd.

KEYWORDS: surface-enhanced Raman spectroscopy; Ag colloids; electrochemical SERS; flavonoids; DFT

INTRODUCTION

Almost all flavone derivatives have been identified from botanical sources.[1] They are commonly found in vascular plants as phenyl-benzopyrones with different basic structures. Many of the flavonoids found in plants exist as sugar derivatives (glycosides).[2] Owing to their active role in photosensitization, energy transport and cellular metabolism, many of flavone derivatives are ingredients for biochemical and pharmacological products used as human diet supplements.[3–8]

Flavones and flavonols found in plants are yellow compounds and are the main components of a number of natural dyes used in textile dyeing since antiquity. Fustic, young fustic, quercitron, Persian berries, weld, dyer's broom and sawwort, which are important yellow dyes, all contain flavonoids such as quercetin, luteolin, fisetin, rhamnetin, genistein and morin.[9] Extracted from plants, they are easily hydrolyzed from the glycosides to their parent flavonoid and can be applied to textiles as mordant dyes.

Despite the fact that flavone forms the parent structure to most flavonoids, there is no Raman or surface-enhanced Raman spectral (SERS) data reported for flavone itself; one of the reasons for this may be the fact that flavonoid derivatives are more abundant in nature and are more extensively used in both medicine and dye industry than plain flavone. Low aqueous solubility may also be a factor. The structures of flavone and of some derivatives are shown in Fig. 1: for convenience in analysis and discussion, we designate the benzo ring in the chromone system as Ring A, the phenyl ring as Ring B and the pyrone ring as Ring C. Some of the previous works provide the infrared spectra of flavone in carbon tetrachloride, dioxane and iodine solutions, and in Nujol boron tetraflouride complex.[10] Studies confirm that the higher wavenumber bands of flavone are dominated by the C═O and C═C vibrations, with bands at 1650, 1621, and 1605 cm^{-1} in CCl_4 and CCl_4-I_2 solutions. The BF_4-nujol and plain nujol spectra confirmed the 1638 cm^{-1} band assignment to C═O and C═C vibrations.

*Correspondence to: John R. Lombardi, Department of Chemistry and Center for Study of Structures and Interfaces (CASI), The City College of New York, New York, N.Y. 10031, USA.
E-mail: lombardi@sci.ccny.cuny.edu
†The first two authors carried out much of the work involved in this research and should be considered equally as principal authors.

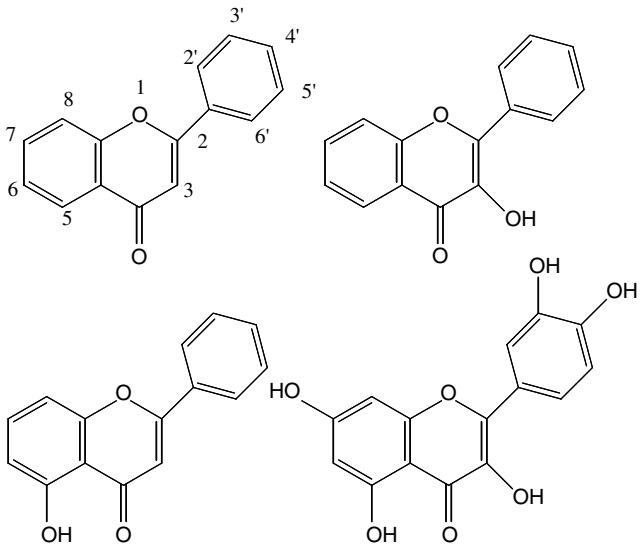

Figure 1. Flavone (upper left), 3-hydroxyflavone (upper right), 5-hydroxyflavone (lower left), and quercitin (3,5,7,3′,4′ pentahydroxyflavone (lower right). For convenience, we designate the benzo ring in the chromone system as Ring A, the phenyl ring as Ring B and the pyrone ring as Ring C.

As a member of flavonoid family, 3-hydroxyflavone (3-HF, flavonol) has been extensively studied for chemical and structural properties by UV, NMR, IR and PMR[11,12] and used in extensive studies of excited-state intramolecular proton transfer and photoisomerization by means of electronic spectroscopy and time-resolved fluorescence measurements.[13–15] Infrared spectroscopy has been widely applied to study the vibrational modes of 3-HF.[16–20] Unlike in flavone where the carbonyl absorption is at 1649 cm^{-1}, in 3-HF its wavenumber is lowered to 1610 cm^{-1} which overlaps with the C═C band. The IR spectra in the C–H and *O*–H stretching region were reported differently in various works,[10,15,16] in which researchers concluded that there is no strong hydrogen bonding in 3-HF, as opposed to the 5-hydroxyflavone (5-HF) molecule. The hydroxyl stretching absorption was found at 3350 cm^{-1}.

Many studies have been reported on 5-HF, including IR, UV, NMR and proton-transfer fluorescence spectra.[10,15,21–23] The published IR spectra show that although in 5-HF the hydroxyl stretching band is broadened and displaced to lower wavenumbers (3000–2500 cm^{-1}) to an extent that it has almost disappeared, none of the compounds examined shows a marked lowering of the carbonyl wavenumber. Two possible canonical forms of 5-HF were reported, which explained the electronic behavior of the molecule and confirmed that the hydroxyl group forms a strong hydrogen bond between the phenolic hydrogen atom and the negatively charged carbonyl oxygen atom. Carbonyl IR absorptions of 5-HF on KBr disk, Nujol mull, CCl_4 and dioxane solution were reported at 1653, 1651, 1652 and 1654 cm^{-1}, respectively. Solid-state IR spectroscopy revealed 5-HF vibrational modes with wavenumbers at 1617, 1590, 1550, 1473, 1457 and 1417 cm^{-1}, which are possibly associated with in-plane skeletal vibrations.[15] Common bands in the 1400–1000 cm^{-1} region have also been studied. Examination of the double bond region revealed C═C and C═O wavenumbers at 1620 and 1612 cm^{-1}, respectively.[10]

One of the most biologically active and common dietary polyhydroxy-substituted derivative of flavonol, quercetin (3,5,7,3′,4′ pentahydroxyflavone Fig. 1), has been studied more extensively than any other flavonoid owing to its complex chemical structure and unique properties. Quercetin and its glycoside quercitrin are the main components of the natural dyestuff quercitron, extracted from the bark of the quercitron, or black oak (*Quercus velutina* Lam.); quercetin is also found in Persian berries, a dye derived from the berries of shrubs of the *Rhamnus* genus.[10] Raman, IR and pulse radiolysis techniques were successfully used to study the chelation properties of quercetin with Cu(II) ions.[24] The double bond region showed the C═O band at 1649 cm^{-1} and the C═C band at 1607 cm^{-1}. X-ray diffraction investigations reported the bond lengths, bond angles and torsional angles of quercetin, which suggested that the conformational changes with the physical state of the molecule are limited to an inter-ring link.[25] FT-Raman spectra of quercetin in the solid state and in solution have shown structural changes in the molecule depending on its physical state. Calculated and experimental wavenumbers[24] were compared after scaling the calculated values by a factor of 0.85 in the region between 600 and 1800 cm^{-1}. UV spectra also supported the calculated wavenumbers of quercetin.

Besides the wide studies on quercetin, there is almost no Raman or SERS work reported on flavone and 3- and 5-HF. A reference to unpublished work by Petroski *et al*.[26] reported 3-HF Raman bands at 1650 and 1625 cm^{-1}. The reason for the lack of Raman work may be the fact that these molecules are poorly soluble in water and show strong fluorescence upon excitation, which tends to obscure the normally weak Raman spectra. Recent studies suggest valuable application of SERS to microscopic samples in the detection of molecules at extremely low concentration, which is particularly valuable in continuing research on biosensors,[27] forensics[28] and art preservation.[29] In collaborative studies with the Metropolitan Museum of Art, we turned our interest to Raman spectroscopy of several natural dye constituents, with an eye toward possible applications in the analysis of works of art. We feel it is likely that Raman spectroscopy will be an efficient technique in the measurement of vibrational modes of flavone, 3-HF, 5-HF and quercetin at milli-, micro- and even nanomolar solutions. Furthermore, a detailed vibrational study and comparative analysis of these molecules could be useful to reveal the effects of hydroxy group substituents on structural and chemical changes of flavones. In this article we report Fourier-transform Raman (FTR) spectra of all four molecules in the solid state as well as their SERS spectra in solution on

DOI: 10.1002/jrs

an Ag colloid and, where possible, on an Ag electrode. All spectral assignments were aided by density functional theory (DFT) calculations. We provide a comparative analysis of the spectra of all molecules of this study in relation to each other. This article will be the base for our future studies of other flavonoids, with the eventual aim of building a reference database of spectral assignments for most of the important derivatives. This database should be of great value in the development of pharmacological and art conservation studies.

In the next section we present details of our experimental procedure, as well as DFT calculations. Following that, we present the analysis of the spectra of flavone, 3-HF, 5-HF and quercetin. The normal mode spectral assignments were aided by DFT calculations, and we compare the results of both the normal Raman (NR) spectrum and SERS spectra. We will then provide a comparative analysis of several of the normal modes of each molecule, showing the effect of various hydroxy substituents on the basic flavone wavenumbers. In the final section, we present a proof-of-concept experiment to demonstrate the feasibility of employing SERS in the analysis of a textile dyed with the natural dyestuff Persian berries, which consists mainly of quercetin.

EXPERIMENTAL

The experimental setup for NR and electrochemical SERS studies has been described in previous papers.[30] A Spectra Physics Model 2020 BeamLock argon ion laser line at 488 nm was used as the Raman excitation source. The spectra were recorded with a Spex Model 1401 double monochromator with a resolution of 2 cm^{-1}. Photon-counting detection was used. The laser power was approximately 30 mW in the SERS experiment but only 5 mW in the NR experiment. Chemicals were purchased from the Aldrich Chemical Company Inc., and used as received.

The NR spectra of the solids were obtained in the region 100–4000 cm^{-1} directly from the pure powder samples. When possible, the 488 nm laser and Raman spectroscopy setup described above were used. In cases where the fluorescence of the dyes prevented the acquisition of a Raman spectrum, FT-Raman spectroscopy was carried out using a Bruker Ram II FT-Raman-Vertex 70 FT-IR microspectrometer. The 1064 nm line of a Nd:YAG laser was used as the excitation line. The resolution was set to 4 cm^{-1} in the backscattering mode. A liquid-nitrogen-cooled Ge detector was used to collect 100 scans for obtaining a good Raman spectrum. The laser output was kept at 150 mW for the SERS spectra and 50 mW for the solid samples.

Additionally, some SERS work on Ag colloids was carried out using a Bruker Senterra Raman microscope using 785 nm excitation with power at the sample ranging from 10 to 100 mW, a 1200 rulings/mm holographic grating and a CCD detector.

The SERS spectra in an electrochemical cell were obtained at different applied potentials with an activated Ag electrode, which had various molecules adsorbed on it. In the SERS experiments, the sample cell consisted of a 99.999% pure silver working electrode, a Pt counter electrode and a saturated calomel electrode (SCE) as the reference. All potentials reported in this paper are quoted *versus* the SCE. For activating a Ag electrode, the polished Ag electrode was roughened by an oxidation–reduction cycle (ORC) pretreatment, which was accomplished in the solution of the flavone molecules (2×10^{-5} M) in 0.1 M K_2SO_4 aqueous solution by applying a potential pulse from −0.4 to 0.5 V for 2 s. These solutions were made with doubly deionized, quartz distilled water. The molecule was adsorbed on the Ag electrode surface during the ORC. Non-adsorbed molecules were then washed from the electrode by distilled water. After the *ex situ* ORC pretreatment, the activated Ag electrode was placed in 0.1 M K_2SO_4 aqueous solution for carrying out SERS experiments at various potentials. The same spectra were also obtained with *in situ* ORC and direct recording of the SERS spectra in the flavone solutions. The ORC pretreatment and potential control during the SERS experiments were carried out by using an EG&G PARC Model 175 universal programmer and an EG&G PARC Model 173 potentiostat.

The Ag colloid was prepared following the method of Lee and Meisel[31] by reduction of silver nitrate (Aldrich 209139 silver nitrate 99.9%) with sodium citrate (Aldrich W302600 sodium citrate dihydrate). The colloid thus prepared shows an absorption maximum at 406 nm and FWHM of 106 nm, as measured with a Cary 50 UV–vis spectrophotometer (after a 1:4 dilution with ultrapure water to keep the maximum absorbance within the instrumental range). To further concentrate the colloid for use, a volume of 10 ml of the original colloid was centrifuged at 5000 rpm for 2 min. The supernatant was discarded and the settled portion was resuspended in 1 ml of ultrapure water. All glassware was cleaned with Pierce PC54 cleaning solution and rinsed with ultrapure water and finally in acetone and methanol. This method proved to be as effective as the use of aggressive cleaning agents such as aqua regia or piranha solution, and was preferred for health and safety reasons. Only ultrapure water was used for the preparation of the various solutions. SERS measurement were made simply by adding 1 μl of the dye solution to a 2 μl drop of the colloid deposited on a gold coated microscope slide, followed by addition of 2 μl of a 0.2 M KNO_3 solution. Raman measurements were made directly from the drop using a 10 or 20× microscope objective and focusing on the microscope slide surface. SERS spectra could be obtained 2 or 3 min after addition of the KNO_3 and remained constant in quality until the evaporation of the liquid.

DFT calculations were performed with Gaussian 03[32] at the B3LYP level of theory and employing the 6-31+G* basis set. The geometry optimization resulted in a planar geometry, and no imaginary wavenumbers were observed

DOI: 10.1002/jrs

in the calculated spectrum. This basis set was chosen to be consistent with earlier work, in which the fit obtained was excellent (see below). We also tried using the basis 6-311G*, which gave an equally good wavenumber fit but with lesser ability to reproduce intensities, which shows the effect of the diffuse functions in the calculation. This was especially true, for example, with the 1544 cm^{-1} line of quercitin, which is intense in the spectrum and using the former calculation, but is quite weak in the latter calculation. A further exploration using the hybrid functional PBE0 and 6-31+G* basis set was carried out for quercitin. This gave essentially the same results as the B3LYP/6-31+G* calculation, but required considerably more computer time and memory. In general, the vibrational normal mode assignments were based on the best-fit comparison of the calculated Raman spectrum with the observed NR spectrum. Where needed, a slight scaling of the calculated spectrum was utilized (usually 0.96–0.99). In instances where there was spectral congestion, such as in the carbonyl stretch region (near 1600 cm^{-1}), the relative intensities of the calculated spectra were matched to those of the observed spectra, so that the most intense calculated lines were assigned to the most intense observed lines.

RESULTS

Flavone

The NR spectrum of solid flavone along with the calculated DFT spectrum is shown in Fig. 2 (200–1800 cm^{-1}). The wavenumber scale of the DFT spectrum was scaled by a factor of 0.98 in order to obtain the best fit of the calculated spectrum with the experimental one. The observed and calculated wavenumbers are listed in Table 1. In the low wavenumber region, we observe an excellent match of the spectrum with the calculated modes. The most intense peaks are well fitted (such as the modes ν_{15}, ν_{17} and ν_{22}). Only a few of the calculated wavenumbers do not match the observed ones in the low wavenumber region, such as at 745 and 888 cm^{-1}. This may be explained by the fact that the signal-to-noise ratio in this region is low and therefore the assignments are uncertain. In the higher wavenumber region, almost all the intense lines correspond to the calculated features. The most intense peak in the spectrum at 1634 cm^{-1} corresponds to the ν_{65} mode calculated at 1627 cm^{-1}. Nearby is also an intense line at 1603 (ν_{63}) cm^{-1}. Both these are assigned to a combination of C═O and C_2═C_3 stretching vibrations. The intense lines at 1621 (ν_{64}) and 1570 (ν_{60}) cm^{-1} are due to in-plane ring stretching combined with a C_4–O stretch.

The colloid spectrum of flavone is shown in Fig. 3 (200–1800 cm^{-1}) along with the NR spectrum. We have also taken a spectrum of the plain reduced citrate colloid (Fig. 4) as a background.[33] This shows that several of the bands observed in the flavone-colloidal spectrum, namely, peaks at 225, 952, 1030 and 1403 cm^{-1}, correspond to citrate vibrations. Despite the background interference, the peaks of flavone vibrations are still intense enough to show a good fit

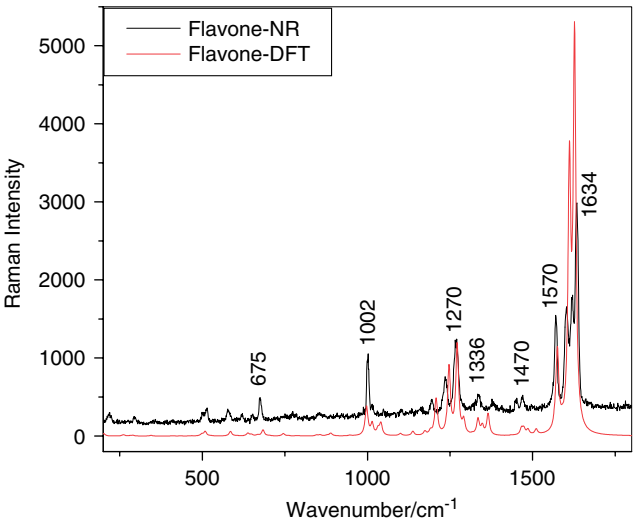

Figure 2. Normal Raman spectrum of flavone powder (dark) and density functional theory calculation (light). This figure is available in colour online at www.interscience.wiley.com/journal/jrs.

with the Raman spectrum of the solid compound. Some of the best matches are at 675, 1002 and 1195 cm^{-1}. In the carbonyl region, however, we observed weakened relative intensity of C═O and C_2═C_3 stretch in the colloid spectrum of flavone compared to a higher intensity of solid flavone, as mentioned above. In the NR spectrum, it will be recalled, these are the most intense peaks, while on the colloid, they are not significantly stronger than many other observed peaks. This is probably due to a weak attachment of the rings of the flavone molecule to colloidal particles. However, as we will notice for the other molecules in this study, much stronger SERS spectra are observed than for the flavone. They are in fact so strong that the colloid background lines observed in the flavone are obscured. Furthermore, after repeated attempts, no spectrum of the flavone on a silver electrode could be observed, although this was easily observed in the other molecules. We interpret this to mean that the presence of an OH group in the 3- or 5-position facilitates strong chemical binding to the Ag surface, which is not possible in the unsubstituted flavone, leading to a relatively weak SERS spectrum.

3-Hydroxyflavone

According to previous IR results,[15–19] the presence of a hydroxy group in the 3-position lowers the wavenumbers of both the carbonyl and C_2═C_3 stretching modes, so that the band at 1610 cm^{-1} in FT-IR (1594 cm^{-1} in NR and SERS) represents the decreased double bond character of the carbonyl group and the aromatic character of the pyrone ring, i.e. the overlapping of C═O with C═C. The band at 3070 cm^{-1} in the NR spectrum can be attributed to an unsaturated C–H stretch. The band at 1351 cm^{-1} in FT-IR (1352 cm^{-1} in NR and 1354 cm^{-1} in SERS) is attributed to an *O*–H in-plane deformation. The bands in the region from

DOI: 10.1002/jrs

Table 1. Wavenumbers (in cm^{-1}) and assignments of the Raman and SERS spectrum of flavone. The DFT wavenumbers are scaled by a factor of 0.98

Mode no.	Description of modes (flavone)	DFT (0.98) (cm^{-1})	Calc. Int.	NR (cm^{-1})	Colloid (cm^{-1})
6	Ring C, C–C deformation (oop)	202	0.1	–	–
7	Rings B, A and C stretch (ip)	262	6	–	–
8	Rings A, B deformation; Ring C═O deformation (oop)	282	0.9	–	–
9	Ring C; C–O bending (ip)	290	2	295	–
10	Ring B, bending; Ring C: C–O bending (ip)	321	2	–	346
11	Ring B, deformation (oop)	411	0.7	–	–
12	Ring C, C – C deformation (oop)	434	0.4	–	449
13	Ring A, B and C, deformation (oop)	467	0.5	–	–
14	Ring C, deformation (ip)	498	5	501	–
15	Ring A, B, C, C–C deformation	509	12	511	–
16	Ring A and C, deformation (oop)	526	0.5	–	520
17	Ring A, B, C, C–C deformation	585	12	577	564
18	Ring A, B and C deformation (ip)	606	0.8	621	614
19	Ring B, deformation (ip)	638	7	652	–
20	Ring A and B, CH bending; Ring C, C2 bending (oop)	649	4	–	–
21	Ring C, CH bending; Ring A and C, deformation (oop)	667	3	–	–
22	Ring A, B and C, deformation (ip)	684	15	675	680
23	Ring CB, C–C deformation	703	1	–	–
24	Ring A, B, C, C–C deformation	745	6	–	746
25	Ring A, B C–H (oop) bend	761	0.9	–	–
26	Ring A, B and C, C–H bending	785	0.8	–	–
27	Ring A, B C–H (oop) bend	792	0.7	–	802
28	Ring A, B, C, C–C deformation	846	2	–	838
29	Ring B, C2′, C3′, C5′, C6′; Ring C, C3 bending (oop)	857	3	856	–
30	Ring A, B and C deformation (oop)	878	2	–	–
31	Ring C, C2–O stretch; Ring A and B deformation (ip)	888	5	–	–
32	Ring A, C–H (oop) bend	891	3	–	–
33	Ring B, bending (oop)	947	1	–	929/952
34	Ring A, C–H bending (oop)	984	0.2	–	–
35	Ring B, C–H (oop) bend	992	2	–	–
36	Ring A, B and C, C–C stretch	998	74	1002	1005
37	Ring A, C–H (oop) bend	1012	0	–	–
38	Ring B, deformation; Ring A and C, C–C stretch	1014	27	1013	–
39	Ring B, C–H bending (oop)	1016	3	–	–
40	Ring A and B, C–C stretch (ip)	1032	16	1032	1030
41	Ring B, C–H (ip) bend	1041	30	1048	–
42	Ring B, C–C stretch (ip)	1094	0.4	–	1098
43	Ring A, deformation; Ring B, C–C stretch (ip)	1101	5	1100	–
44	Ring A, C–H (ip) bend	1138	11	1143	–
45	Ring A, C–C stretch (ip)	1174	9	1162	1170
46	Ring B, C–H (ip) bend	1191	10	–	–
47	Ring B, C–H (ip) bend	1207	74	1195	–
48	Ring A and B, C–C stretch; Ring C, C–O1 stretch	1209	22	–	–
49	Rings A and C, C–C (ip) def	1247	174	1235	1244
50	Ring A, B and C, C–H bending (ip)	1271	232	1270	1256
51	Ring A and B, C–H (ip) bend;	1292	34	–	–
52	Ring A and B, C–H (ip) bend;	1318	2	–	–
53	Ring A, B and C, C–C stretch	1335	40	1336	1322
54	Ring A and B, C–H (ip) bend;	1348	22	–	–

(*continued overleaf*)

DOI: 10.1002/jrs

Table 1. (*Continued*)

Mode no.	Description of modes (flavone)	DFT (0.98) (cm^{-1})	Calc. Int.	NR (cm^{-1})	Colloid (cm^{-1})
55	Ring A, CC trigonal stretch	1365	54	1377	1359
56	Ring B, CH (ip) bend;	1466	16	1452	1403
57	Ring A, CH (ip) bend	1473	15	1470	–
58	Ring A, CH (ip) bend	1486	13	–	–
59	Ring B, CH (ip) bend;	1509	13	–	1522
60	Ring A, B, and C, C–C and C4–O stretch (ip)	1573	28	–	–
61	Ring A, quinoid stretch; C=O stretch	1575	195	1570	1556
62	C=O stretch; in-phase-C2=C3 stretch	1589	10	–	–
63	Ring B, quinoid stretch	1589	664	1603	1603
64	Ring A, B, and C, C–C and C4–O stretch (ip)	1621	12	1621	1625
65	C=O stretch; out-of-phase C2=C3 stretch	1627	994	1634	1636
66	Ring A and B, CH stretch	3106	–	3075	2929
67	Ring A and B, CH stretch	3113	–	3075	2929
68	Ring A and B, CH stretch	3115	–	3075	2929
69	Ring A and B, CH stretch	3119	–	3075	2929
70	Ring A and B, CH stretch	3130	–	3075	2929
71	Ring A and B, CH stretch	3130	–	3075	2929
72	Ring A, CH stretch (ip)	3143	–	3075	2929
73	Ring B, CH stretch	3143	–	3075	2929
74	Ring B, CH stretch (ip)	3154	–	3075	2929
75	Ring C, C3–H stretch (ip)	3160	–	–	–

ip: in-plane; oop: out-of-plane.

1400 to 1600 cm^{-1} are associated with aromatic in-plane skeletal vibrations, double bond character of the carbonyl group and the aromatic character of the pyrone ring, i.e. the overlapping of C=O with C=C.

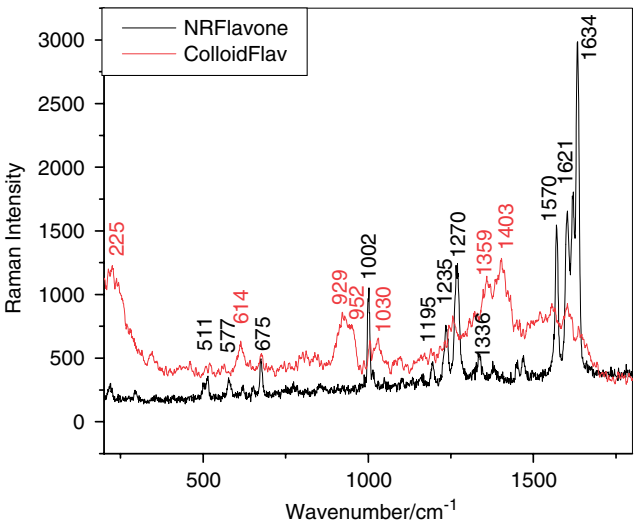

Figure 3. Comparison of the normal Raman with the colloid SERS spectrum of flavone in the region 200–1800 cm^{-1}. This figure is available in colour online at www.interscience.wiley.com/journal/jrs.

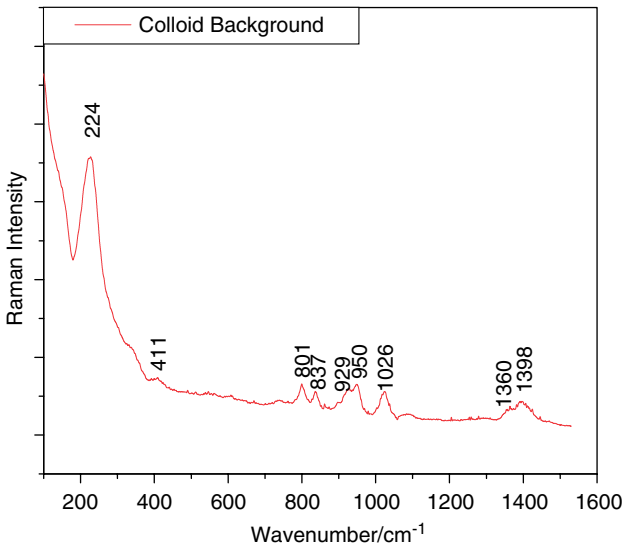

Figure 4. The colloid-citrate background. This figure is available in colour online at www.interscience.wiley.com/journal/jrs.

The Raman spectra of 3-HF have been considered in more detail in previous studies.[34,35] To facilitate comparison with the other molecules, we have abstracted some of the results here. In Fig. 5 we compare the results of the NR spectrum of the powder sample with the spectrum calculated

DOI: 10.1002/jrs

from the DFT results. Detailed measured wavenumbers and the calculated wavenumbers are listed in Columns 3 of Table 2. The raw wavenumbers from the calculation have been adjusted by a factor of 0.98. It can be noticed that the calculated spectrum provides an excellent fit to the observed result. This indicates that the assignments given in the first two columns of the table are most likely correct. In Column 1 we provide the normal mode identification number from the DFT calculation, and in Column 2 we provide a brief description of the largest vibrational contributions to the normal mode. Most of the lines between 1305 and 1509 cm^{-1} involve the in-plane CH bending vibration. Note also that, except for the band at 1594 cm^{-1} (ν_{64}), all the bands between 1562 and 1619 cm^{-1} involve the C═O stretch and the C_2═C_3 stretch, with some degree of *O*–H bend.

In order to examine the differences between the SERS spectrum on a colloid and that on the electrode, we present both the spectra in Fig. 6. By and large the spectra are quite similar, except that the line at 1527 cm^{-1} (ν_{62}) is very intense on the colloid and weak on the electrode. Furthermore, the 1405 cm^{-1} (ν_{58}) and 516 cm^{-1} (ν_{17}) bands are similarly much stronger on the colloid. The latter vibration involves C–C in-plane deformation of the three rings, while the two at higher wavenumbers are due to C–H in-plane bending motions. These higher wavenumber modes also involve C–*O*–H bending, and a much stronger interaction on the electrode of a positively charged Ag ad-ion with the oxygen atom of the C–O bond in Ring C might damp the Ring C motion.

The most interesting result is illustrated in Fig. 7, in which we compare the NR spectrum of 3-HF with that of the SERS on the colloid in the spectral region between 1000 and 1800 cm^{-1}. We notice immediately that the intense NR

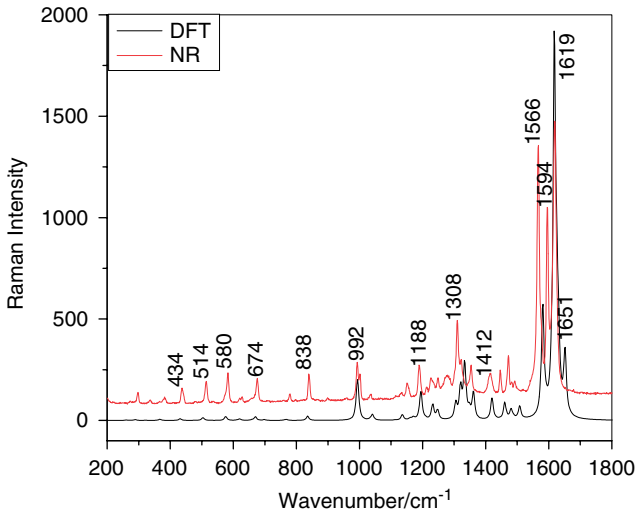

Figure 5. Comparison of normal Raman spectrum and density functional theory calculation for 3-hydroxyflavone in the region 200–1800 cm^{-1}. This figure is available in colour online at www.interscience.wiley.com/journal/jrs.

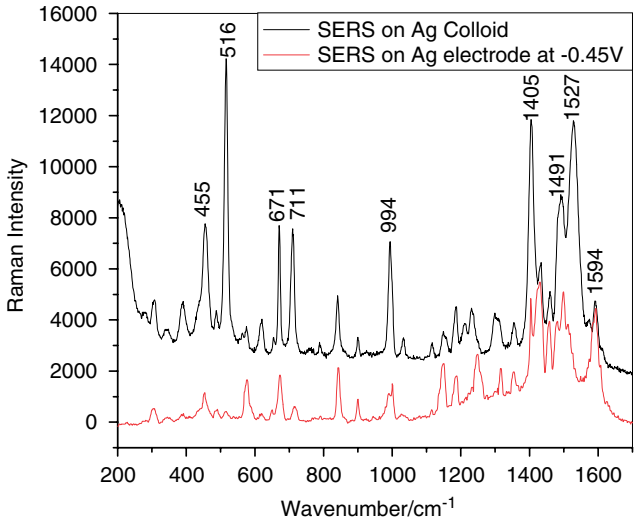

Figure 6. Comparison of SERS spectrum of 3-hydroxyflavone on a silver colloid with that on a silver electrode at −0.45 V. This figure is available in colour online at www.interscience.wiley.com/journal/jrs.

bands at 1566, 1594 and 1619 cm^{-1} (ν_{63}–ν_{65}) are suppressed on the surface, whereas the lines at 1405, 1491 and 1527 cm^{-1} (ν_{58}, ν_{61}, ν_{62}) become the most intense lines in the spectrum. The suppressed lines have either a strong C═O stretch coupled with a C_2═C_3 stretch or an *O*–H bend, while the surface-enhanced lines all involve the C–H in-plane wag. These results (in addition to the concomitant results on the Ag electrode) indicate strongly that the molecule is attached to an Ag ad-atom on the metal surface, reducing the intensity of the modes involving C═O and C_2═C_3 stretch. The strong enhancement of the C–H in-plane wags indicates that the planar rings involved are oriented perpendicular to the metal surface. This is consistent with the suppression of the 1527 cm^{-1} band in the SERS on the Ag electrode, where an Ag ad-ion could be involved in the bonding of the –OH molecule to the surface. Note also that the lines at 455 (ν_{15}), 516 (ν_{17}), 671 (ν_{24}) and 711 (ν_{27}) cm^{-1} are greatly enhanced on the colloid in comparison to the most intense lines of the NR spectrum. These lines involve in-plane ring C–C deformations. We shall notice a similar result for the remaining two molecules studied here.

5-Hydroxyflavone

In Fig. 8 we show the NR spectrum of the powder form of 5-HF, along with the results of the DFT calculation scaled by a factor of 0.97. Refer to Table 3 for a complete summary of the observed and calculated lines. It can be noticed that with this scaling an excellent fit is obtained. The most intense lines at 1569, 1602, 1610 and 1650 cm^{-1} are assigned to the C═O, C_2═C_3 stretch and the Ring B quinoid stretch, as in flavone and 3-HF.

Figure 9 displays a comparison of the results on a silver electrode at −0.45 V with those on a colloid. For additional

DOI: 10.1002/jrs

Table 2. Wavenumbers (in cm^{-1}) and assignments of the Raman and SERS spectrum of 3-hydroxyflavone. The DFT wavenumbers are scaled by a factor of 0.98

	Density functional calculations (cm^{-1})		NR (cm^{-1})	SERS (cm^{-1})	SERS (cm^{-1})	FT-IR
Mode no.	Description		(Solid)	at −0.45 V	Colloid	(KBr)
10	Ring B, C–OH (ip) rock	321	296	304	307	–
12	C – OH bend; C═O bend	367	380	390	390	–
15	Ring C, C–C deformation	431	434	454	455	–
17	Ring A, B, C, C–C deformation	504	514	516	516	–
19	Ring A, B, C, C–C deformation	576	580	578	575	–
21	Ring B, C–C deformation	619	624	618	620	–
24	Rings A, B, C, C–C deformation	670	674	672	671	–
27	Rings A, C, C–C deformation; C–*O*–C stretch	698	–	712	711	704
28	Rings A, B C–H (oop) bend	731	–	–	–	–
30	Rings A, B C–H (oop) bend	766	780	–	789	775
31	Rings A, B, C, C–C deformation	834	838_s	842_s	842	839_w
33	Ring A, C–H (oop) wag	859	–	–	–	864_m
34	OH Bend; Rings A, B, C, C–C deformation	890	899	900_m	900	898_s
35	Ring B, C–H (oop) wag	923	–	–	–	–
36	Ring A, C–H (oop) wag	956	–	946_{vw}	–	930_w
40	Rings A, B, C, C–C deformation	994	992_s	992_s	994	989_m
41	Rings A, B, C, C–C deformation	996	1000_s	1000_s	–	–
43	Ring B, C–H (ip) wag	1041	1034_w	1028_{vw}	1032	1034_m
44	Ring B, C–H (ip) wag	1091	–	1078_{vw}	–	1078_m
46	Ring A, C–H (ip) wag	1137	1134_w	1116_w	1117	1130_s
48	Ring B, C–H (ip) wag	1170	1148_m	1150_s	1153	1155_w
49	C–OH stretch; Ring B, C–H (ip) wag	1194	1188_s	1186_s	1186	1184_w
50	C–OH stretch; Ring B, C–H (ip) wag	1208	1212_w	1218_{sh}	1213	1211_s
51	Ring C, C–C stretch	1233	1226_m	–	1233	1224_w
52	Rings B and C, C–C (ip) def	1248	1246_m	1248_s	–	1247_w
			1278_m			1286_s
53	Rings A and B, C–H (ip) wag; *O*–H bend	1305	1308_s	1298_{sh}	1299	1306_s
54	Rings A and B, C–H (ip) wag; *O*–H bend	1321	1320_{sh}	1316_s	1316	1321_w
55	O–H (ip) bend	1332	–	–	–	–
57	OH (ip) Bend; Ring A, CC trigonal Stretch	1360	1352_s	1354_m	1355	1351_s
58	Rings A and B, CH (ip) wag; OH Bend	1421	1412_s	1404_s	1405	1416_s
			1444_s	1430_s	1430	1445_m
59	Ring B, CH (ip) wag; OH Bend	1460	1470_s	1457_s	1461	1471_s
60	Ring A, CH (ip) wag	1481	1482_w	1482_{sh}	–	1481_s
61	Ring A, CH (ip) wag	1489	1490_m	1498_s	1491	1491_{sh}
62	Ring B, CH (ip) wag; OH Bend	1509	–	–	1527	–
63	Ring A, ip def; C═O Stretch; OH Bend	1581	1566_{vs}	–	1574_w	1562_s
64	Ring B, quinoid Stretch; OH Bend; C_2═C_3 Stretch	1590	1594_{vs}	1594_s	1592	1602_s
65	C═O Stretch; C_2═C_3 Stretch	1617_{vs}	1619_{vs}	–	–	1610
66	Rings A, B, C ip def	1627	–	–	–	1627_w
68	C═O Stretch; OH Bend; C_2═C_3 Stretch	1651	–	–	–	1647_{vw}
69	Ring B, CH stretch	3119	–	2860_w	–	–
70,71	Rings A and B, CH stretch	3130	–	2910_w	–	–
72,73	Rings A and B, CH stretch	3143	3070_m	3070_{vw}	–	–
75	Ring B, CH stretch	3160	–	3200_{vw}	–	3211_s
78	OH stretch	3420	–	–	–	–

ip: in-plane; oop: out-of-plane.

DOI: 10.1002/jrs

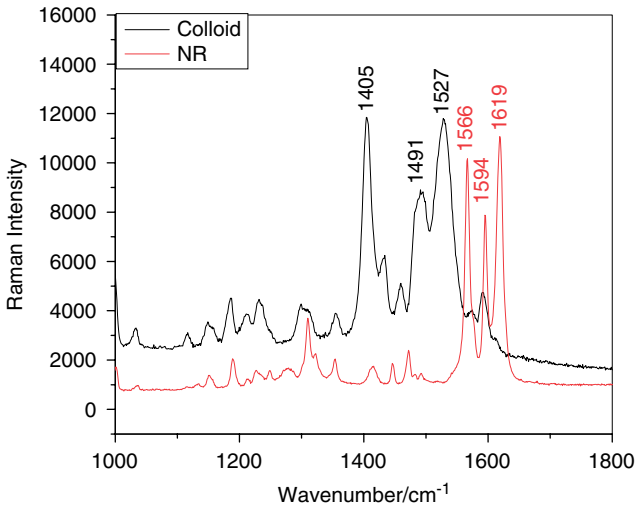

Figure 7. Comparison of the SERS spectrum of 3-hydroxyflavone with the normal Raman spectrum in the region 1000–1800 cm^{-1}. This figure is available in colour online at www.interscience.wiley.com/journal/jrs.

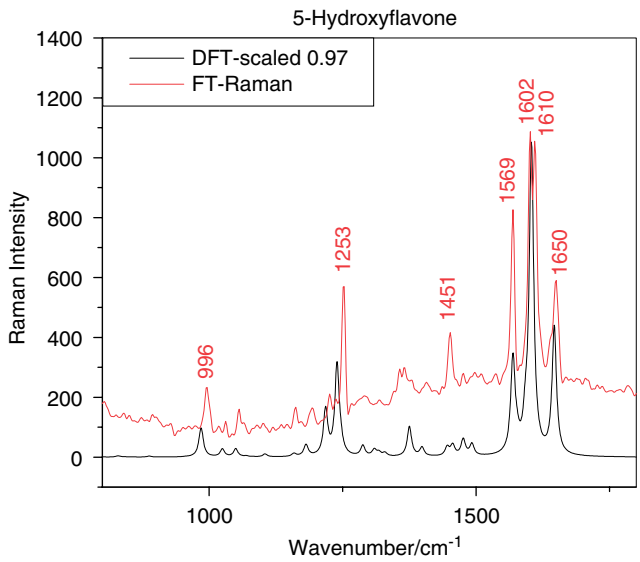

Figure 8. FT-Raman spectrum of 5-hydroxyflavone and comparison with density functional calculation in the region 800–1800 cm^{-1}. This figure is available in colour online at www.interscience.wiley.com/journal/jrs.

clarity, the DFT results are also included. As with flavone and 3-HF, the intensity of the lines near 1600 cm^{-1} are reduced relative to the other lines, especially those near 450–650 cm^{-1} (459 (ν_{16}), 524 (ν_{19}), 560 (ν_{20}), 619 (ν_{21}) and 659 (ν_{22}) cm^{-1}), which rival all the other lines in the spectrum for intensity. These are some of the same modes that were strongly enhanced in 3-HF. In the NR and DFT, these lines are very weak. It is clear that proximity to the surface strongly affects both spectral regions but in opposite directions. The loss of intensity in the C═O stretching region indicates strong

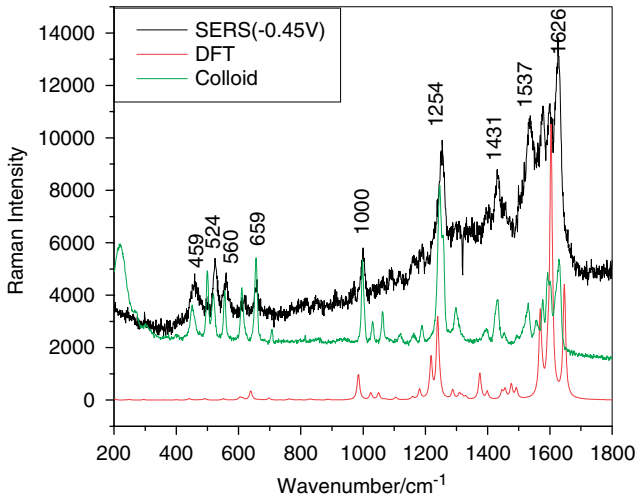

Figure 9. Comparison of SERS of 5-hydroxyflavone on electrode (top), colloid (middle) and DFT (bottom) in the region 200–1800 cm^{-1}. This figure is available in colour online at www.interscience.wiley.com/journal/jrs.

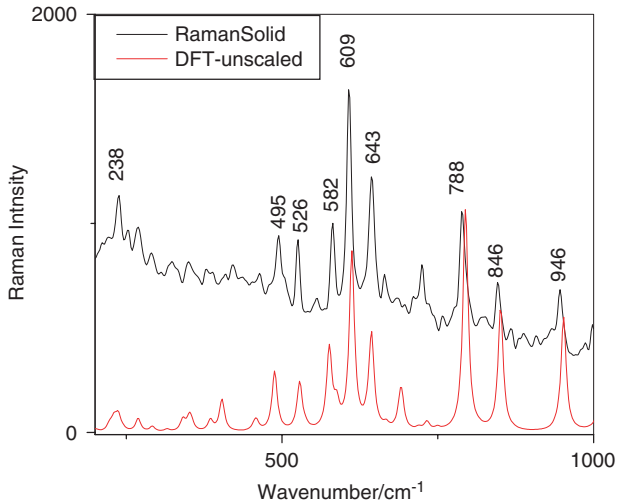

Figure 10. FT-Raman spectrum (200–1000 cm^{-1}) of solid quercitin compared with DFT calculated spectrum (unscaled). This figure is available in colour online at www.interscience.wiley.com/journal/jrs.

attachment of the molecule to the surface for the C═O and OH moieties, while the in-plane C–C deformations, farther from the surface, are clearly enhanced by the fact that their vibrational modes involve motions perpendicular to the surface.

Quercetin

The FT-Raman spectrum of solid quercetin is displayed in Figs 10 (200–1000 cm^{-1}) and 11 (1000–2000 cm^{-1}) along with the results of the DFT calculations. In the low wavenumber region, it was unnecessary to apply a scaling factor to the DFT results in order to obtain a good fit. In the higher

DOI: 10.1002/jrs

Table 3. Wavenumbers (cm^{-1}) and assignments of the Raman and SERS spectrum of 5-hydroxyflavone. The DFT wavenumbers are scaled by a factor of 0.97

Mode	DFT description of modes	Int Calc.	DFT (cm^{-1}) 0.97	5-HF (cm^{-1}) FT-NR	5-HF (cm^{-1}) FT-IR	5-HF (cm^{-1}) Colloid	5-HF (cm^{-1}) SERS-0.45
6	Ring C, C–C deformation (oop)	–	–	224	–	–	–
7	Ring A, C–OH deformation (oop)	1	237	–	–	220	–
8	Ring A, B and C stretch (ip)	2	242	–	–	–	–
9	Rings A, B and C stretch (ip)	2	261	254	–	–	–
10	Rings A, B deformation; Ring C; O deformation (oop)	1	284	291	–	266	–
11	Ring C and B, C–O stretch	2	341	340	–	302	–
12	Ring A, O–H bending (oop); Ring C and B, C – C stretch	4	400	–	–	–	–
13	Ring A, O–H bending (oop)	4	402	–	–	–	–
14	Ring B, deformation (oop)	1	406	–	–	–	–
15	Ring A, B and C, deformation (oop)	0	456	456	–	–	–
16	Ring C and B, C–C bending (ip)	2	477	–	–	451	459
17	Ring A and C, deformation (oop)	1	488	484	–	–	–
18	Ring A, B, C, C–C deformation	5	493	502	–	500	–
19	Ring A, B, C, C–C deformation	4	561	561	–	519	524
20	Ring A, B and C, C–C bending (ip)	16	598	618	–	555	560
21	Ring A and B, CH bending; Ring C deformation (ip)	1	599	–	615	611	619
22	Ring A, B, C, C–C deformation (ip)	21	629	–	–	–	–
23	Ring B, deformation (ip)	9	632	–	–	–	–
24	Ring A, B, C, C–C deformation	3	640	–	–	–	–
25	Ring A, B, C–H (oop) bend	3	654	651	650	657	659
26	Ring A, and C, C–H bending	2	695	708	675	707	–
27	Ring A, B, C–H (oop) bend	2	697	–	688	–	–
28	Ring A, B, C–H (oop) bend	0	751	–	754	–	–
29	Ring A, B, C–H (oop) bend	1	775	776	–	–	–
30	Ring A, B and C, C–H bending	1	783	–	–	–	–
31	Ring A, B, C, C–C deformation	3	800	–	802	814	814
32	Ring B, C_2', C_3', C_5', C_6'; Ring C, C_3 bending (oop)	3	849	–	843	–	848
33	Ring A, C–H (oop) bend	1	861	–	–	–	–
34	Ring C, C_3–H bending (oop)	3	872	–	–	–	–
35	Ring A, B and C deformation (oop)	3	882	–	–	–	–
36	Ring B, C–H (oop) bend	2	936	–	900	–	–
37	Ring A, B and C, C–C stretch	11	945	–	931	–	910
38	Ring A, C–H (oop) bend	0	964	–	–	–	–
39	Ring B, C–H bending (oop)	1	982	–	–	–	971
40	Ring B, deformation; Ring A and C, C–C stretch	96	999	997	997	998	1000
41	Ring B, C–H bending (oop)	1	1005	–	–	–	–
42	Ring A and B, C–C stretch (ip)	1	1021	–	–	–	–
43	Ring B, C–H (ip) bend	2	1034	1032	1032	1030	–
44	Ring A, C–C stretch (ip); Ring B and C C–H bending (ip)	40	1061	1057	1057	1062	1065
45	Ring A, deformation; Ring B, C–C stretch (ip)	1	1083		1083	–	1091
46	Ring A, C–H (ip) bend	3	1108	–	1120	1121	1115

(*continued overleaf*)

DOI: 10.1002/jrs

Table 3. (*Continued*)

Mode	DFT description of modes	Int Calc.	DFT (cm^{-1}) 0.97	5-HF (cm^{-1}) FT-NR	5-HF (cm^{-1}) FT-IR	5-HF (cm^{-1}) Colloid	5-HF (cm^{-1}) SERS-0.45
47	Ring A, C–C stretch (ip)	5	1164	1163	1157	1162	1163
48	C–OH stretch; Ring B, C–H (ip) bend	9	1179	–	–	–	–
49	Ring A, C–H, C–OH bending (ip)	3	1183	–	–	–	–
50	C–OH stretch; Ring B, C–H (ip) bend	57	1194	1195	–	1189	1190
51	Ring A, B and C deformation (ip)	49	1209	1227	–	–	–
52	Ring A, B and C, C–H bending (ip)	365	1252	1253	1257	1255	1254
53	Ring A, C–H bending (ip)	21	1262	–	–	–	–
54	Ring A and B, C–H (ip) bend;	19	1277	–	–	–	–
55	Ring A and B, C–H (ip) bend;	11	1305	1291	1300	1298	1308
56	Ring A, B and C, deformation (ip); C–OH bending (ip)	5	1319	1318	1319	–	–
57	Ring A, B and C, C–C stretch	46	1334	–	–	–	1332
58	Ring A and B, C–H (ip) bend;	48	1349	1357	1365	–	–
59	Ring A, C–C stretch (ip)	25	1440	–	1417	1431	1431
60	Ring B, CH (ip) bend;	18	1452	1451	1452	1453	1458
61	Ring A, CH (ip) bend	7	1478	1475	1475	–	–
62	Ring B, CH (ip) bend;	17	1497	1498	–	1494	1499
63	Ring A, B, and C, C–C and C_4–O stretch (ip)	56	1557	–	–	1557	–
64	Ring A, quinoid stretch; C═O stretch	66	1568	1569	–	1577	1579
65	C═O stretch; in-phase-C_2═C_3 stretch	37	1580	–	1589	–	–
66	Ring B, quinoid stretch	500	1603	1602	–	1593	–
67	Ring A, B, and C, C–C and C_4–O stretch (ip)	69	1613	1610	1622	1600	1600
68	C═O stretch; out-of-phase-C_2═C_3 stretch	105	1646	1650	1657	1629	1626
69	Ring A, C_6, C_7–H stretch (ip)	120	3069	3062	3060	–	–
70	Ring A and B, CH stretch	47	3073	3062	3060	–	–
71	Ring A and B, CH stretch	132	3083	3062	3060	–	–
72	Ring A and B, CH stretch	108	3095	3062	3060	–	–
73	Ring A and B, CH stretch	154	3096	3062	3060	–	–
74	Ring B, C–H stretch (ip)	193	3106	3062	3060	–	–
75	Ring B, CH stretch	118	3124	3062	3060	–	–
76	Ring B, CH stretch (ip)	80	3125	3062	3060	–	–
77	Ring C, C_3–H stretch (ip)	–	–	–	–	–	–
78	O–H stretch (ip)	248	3566	–	–	–	–

ip: in-plane; oop: out-of-plane.

wavenumber section of the spectrum, it was found necessary to multiply the raw DFT wavenumbers by a factor of 0.97 in order to properly fit the observed spectrum. Such piecewise scaling of the DFT results has been found necessary in numerous previous studies.[36–38] The observed wavenumbers and their corresponding assignments are listed in Table 4. The assignments were readily obtained owing to the excellent matching of the DFT calculations with the observed spectrum. We also include in the table results of Cornard *et al*.[25] who first obtained the FT-Raman and IR spectra of quercetin both in solid and solution. They used a single point Hartree-Fock SCF calculation as aid in the assignments. Our observed spectra are in good agreement with their experimental results. However, we present normal mode assignments based on more accurate and optimized DFT calculations, several of which disagree with the earlier results.

In the low wavenumber region (Fig. 10), each of the intense lines corresponds somewhat closely to a calculated feature, and the assignment is clear for these lines. In order to obtain a good fit in the region above 1000 cm^{-1}, as mentioned

DOI: 10.1002/jrs

Table 4. Wavenumbers (in cm^{-1}) and assignments of the Raman and SERS spectrum of quercitin. DFT calculations are scaled by 0.97 unless marked by 'u' for unscaled

Mode no.	DFT	Description	Raman Solid[a] (cm^{-1})	Raman Solution[a] (cm^{-1})	FT-Raman Solid[b] (cm^{-1})	FT-Raman Colloid[b] (cm^{-1})	SERS −0.50 V[b] (cm^{-1})
21	404u	Rings A, C ip rock; $C_{5,7}$ OH bend	–	–	–	420	433
24	460u	Rings A, C ip rock; $C_{3,7}$ OH bend	–	–	–	460	452
25	488u	Ring B, CC ip rock, $C_{3',4'}$ OH bend	–	–	495	481	–
26	528u	Ring A, CC ip def	–	–	526	–	521
28	576u	Ring A, B CC ip def	–	–	582	586	582
32	612u	Ring A, B, C ip CC def	604	601	609	605	608
34	643u	Ring A, B ip CC def	640	638	643	636	–
35	667u	Ring A, B, C oop CC, CH bend	661	666	665	–	662
36	689u	Ring A, B, C oop CC, CH bend	686	687	–	–	676
38	719u	Ring A, B ip CC def	721	–	724	722	711
42	794u	Ring B, ip C═C str	785	789	788	772	–
46	851u	Rings A, B, C ip CC str	843	845	846	846	845
49	952u	Rings A, B, C ip CC str	942	938	946	954	–
50	1013u	CH ip bend, C–O–C bend	1013	–	998	–	1002
53	1130u	3,3′,4′ O–H, CH bend	–	–	1116	1100	1115
54	1139u	CH, OH, ip bend	–	–	1139	–	1149
55	1179u	C_7OH, C_8H ip bend	1175	1170	1178	1199	1186
59	1219u	CH ip bend	1216	1209	1222	–	–
60	1263u	CH, OH ip bend	–	–	1266	1255	1253
61	1266u	CH, OH ip bend	1268	1267	–	–	–
64	1310	3,5,3′ OH ip bend	1315	1321	–	–	1319
66	1321	3 OH bend	1328	1333	1332	1338	1338
67	1343	4′ OH bend, CH ip bend	1357	1346	–	–	1355
68	1362	3,5,7 OH ip bend	1371	1376	1372	–	–
69	1386	3,5,7 OH ip bend	1398	1402	1403	1401	1406
70	1414	OH, CH ip bend, Rings A, B, C CC	1410	1419	–	–	–
71	1432	3,5,7 OH bend, Ring A CC, B C═C	–	1431	–	–	1433
72	1466	3,5 OH, CH ip bend, C═O	1440	1447	1444	–	–
73	1489	3,5,7 OH ip bend $C_{6,8}$ H ip bend	1463	1464	–	1459	1461
74	1517	Ring B, CH ip bend	1531	1501	–	1500	1500
75	1551	C═O str, 5 OH bend, Ring B CC str	1548	1569	1544	–	–
76	1585	C═O str, OH ip bend, Ring A B CC	1596	1577	1588	1594	1598
78	1599	C═O, C_2═C_3 str, 3, 5 OH bend	1604	1613	1604	–	–
79	1617	C_2═C_3 str, 3, 5 OH bend	1609	1627	–	–	–
80	1638	5 OH bend, Ring A quinoid str	1662	1656	1660	1644	
81	3058	C5′–H str	–	–	3042	–	3042
82	3084	C4–H str	–	–	3081	–	3072
83	3094	C2′–H str	–	–	3114	–	–
84	3123	C8–H str	–	–	–	–	–
85	3158	C6′–H str	–	–	–	–	–
86	3283	5 OH str	–	–	–	–	–
87	3475	3 OH str	–	–	–	–	–
88	3670	3′,4′ OH str (asym)	–	–	–	–	3699
89	3671	7 OH str	–	–	–	–	3714
90	3675	3′,4′ OH str (sym)	–	–	–	–	3784

ip: in-plane; oop: out-of-plane;

[a] Ref. 25.

[b] This work.

DOI: 10.1002/jrs

above, it was necessary to scale the DFT results by a factor of 0.97. Once again, in this case an excellent fit is obtained. The most intense region of the spectrum is around 1600 cm^{-1}, which usually involves the C═O stretching modes among others. At still higher wavenumbers (~3000 cm^{-1}), only a single line is observed at 3081 cm^{-1}, which is the C–H stretching region (predicted to be between 3058 and 3158 cm^{-1} (scaled) in the DFT). This line is set atop a broad featureless band. Despite the DFT predictions of various *O*–H stretching bands between 3283 and 3675 cm^{-1}, none was observed in the spectrum, possibly owing to interactions with adjacent molecules in the crystal.

The most intense line in the FT-Raman spectrum of the solid is that at 1604 cm^{-1}, which is assigned to the ν_{78} mode (1599 cm^{-1} in the calculation). This may be described as mainly a combination of the C═O stretch, C_2═C_3 stretch and in-plane 3 and 5 *O*–H bends. The nearby ν_{75} (at 1544 cm^{-1}) is somewhat weaker and is assigned as the C═O stretch, the 5 *O*–H (in-plane) bend and the Ring B, C═C deformation. The ν_{80} mode (at 1660 cm^{-1}) involves the 5 *O*–H bend and the Ring A, quinoid stretch. This region closely resembles that of the most intense lines in the corresponding spectrum of flavone and its 3- and 5-hydroxy derivatives discussed above. In those spectra, the most intense lines also tended to involve the C═O stretch. By examining the assignments of quercetin, it is clear that the in-plane *O*–H bends are responsible for a plurality of the observed spectral lines. Part of this is clearly just due to the fact that there are five hydroxy substituents, and these would be expected to have a noticeable effect on the spectrum.

In Fig. 12, we show a comparison of the spectrum of solid quercetin with that of quercetin adsorbed on a silver colloid and on an Ag electrode at −0.50 V. The measured wavenumbers are listed in Table 4. Note that the wavenumbers of a majority of the lines are the same, while the intensities of many lines are changed by proximity to the metal surface, as is common in SERS. Especially noteworthy is the observation of the shift of the 1660 cm^{-1} line (ν_{80}) to 1644 cm^{-1} in the colloid, with little loss of relative intensity. The rather large shift indicates that this is a likely site for adsorption to the surface. On the electrode this line is not noticed, or is perhaps hidden in the rather large shoulder that is commonly observed on Ag electrodes in this region. The line at 1544 cm^{-1} (ν_{75}), also involving the C═O stretch, disappears, possibly for the same reason. On the other hand, the band at 1588 cm^{-1} (ν_{76}) is only slightly shifted to 1594 cm^{-1} on the colloid and 1598 cm^{-1} on the electrode, also with little loss in intensity. Note also that several lines involving various in-plane OH and CH bends (such as 1100 (ν_{53}), 1199 (ν_{55}), 1255 (ν_{60}) and 1338 (ν_{66})) are strongly enhanced on the colloid surface. On the electrode, still other lines are strongly enhanced (i.e. at 1002 (ν_{50}), 845 (ν_{46}), 676 (ν_{36}) and 452 (ν_{24}) cm^{-1}).

Note, however, that the most intense lines, i.e. those at 420, 460, 481, 1459 and 1500 cm^{-1}, in the SERS spectrum

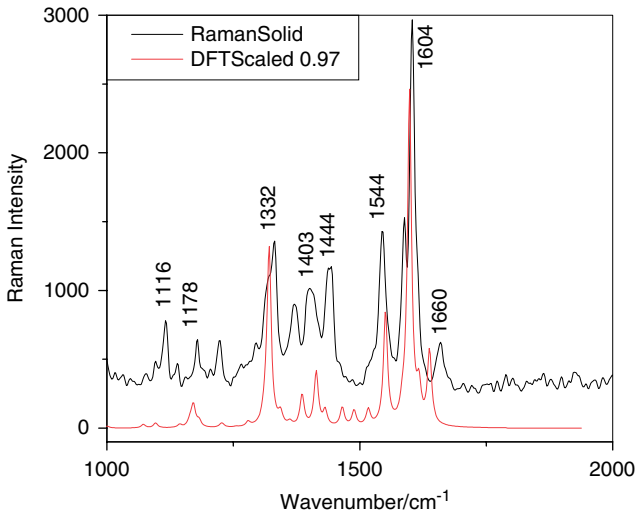

Figure 11. FT-Raman spectrum (1000–2000 cm^{-1}) of solid quercitin (upper) compared with DFT calculated spectrum (lower) with wavenumbers scaled by 0.97. This figure is available in colour online at www.interscience.wiley.com/journal/jrs.

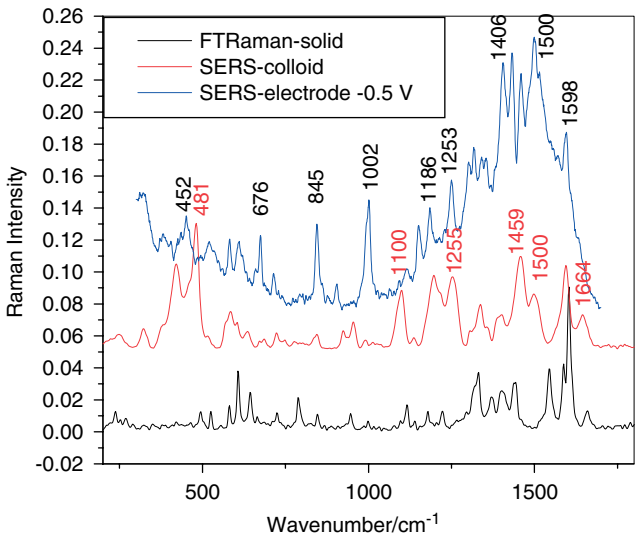

Figure 12. FT-Raman spectra of quercitin in solid (lower) on Ag colloid surface (middle) and on Ag electrode at −0.50 V (upper). This figure is available in colour online at www.interscience.wiley.com/journal/jrs.

on the colloid are strongly enhanced compared to those in the NR spectrum. These lines are also predicted to be weak by the DFT calculations. The lowest three are assigned to in-plane ring deformations, but with a strong component of C–OH in-plane bending. For example, the line at 420 cm^{-1} (ν_{21}) has a strong C_5OH and C_7OH bend, while the line at 481 cm^{-1} (ν_{25}) has strong contributions from $C_{3'}$ OH and $C_{5'}$ OH bends. The line at 1459 cm^{-1} (ν_{73}) involves 3, 5 and 7 OH in-plane bends, while that at 1500 cm^{-1} (ν_{74}) is composed of

DOI: 10.1002/jrs

Table 5. Comparison of C═O stretching region for flavone, 3-hydroxyflavone and 5-hydroxyflavone (Fig. 13). Note the ν_{66} mode in 3-HF is not noticed in the spectrum, so we substituted the calculated (scaled) wavenumber in parentheses

Flavone (cm^{-1})	3-HF (cm^{-1})	5-HF (cm^{-1})	Mode description
1570 ν_{61}	1566 ν_{63}	1569 ν_{64}	Ring A ip def, C═O stretch
1603 ν_{63}	1594 ν_{64}	1602 ν_{66}	Ring B quinoid stretch
1621 ν_{64}	(1627) ν_{66}	1610 ν_{67}	Rings A, B, C deformation (ip)
1634 ν_{65}	1619 ν_{65}	1650 ν_{68}	C═O, C_2═C_3 stretch

ip: in-plane.

Table 6. Modes of 3- and 5-hydroxyflavone, which are strongly enhanced on the colloid surface (Fig. 15)

3-HF (cm^{-1})	Mode no.	5-HF (cm^{-1})	Mode no.	Description (DFT)
711	27	707	26	Ring B, C def, CH ip bend
671	24	657	23	Ring A, B def
620	21	611	21	Ring C, def
575	19	555	20	Ring A, B, and/or C def
516	17	519	19	Ring A, B, and/or C, def
488	16	500	18	Ring A, and/or C, def
455	15	451	16	Ring A, B, and/or C def

ip: in-plane.

Ring B in-plane CH bends. The strongly enhanced intensity of these lines is clearly a result of interaction with the surface. However, the most strongly enhanced lines on the Ag electrode mainly involve in-plane ring stretches. It is possible that the potential on the colloid is quite different from that on the electrode. We also note that the colloid has a coat of citrate remaining. These may account for the differences, and a study of the complete potential dependence of the SERS would be in order. Furthermore, we cannot rule out the possibility of a photoproduct. For example, Sanchez-Cortes *et al.*,[39] in studies of diphenols on Ag colloids, found several new Raman bands, which they attributed to production of dimers through formation of C–C and either C–*O*–C bonds between pairs of diphenols. However, further investigations are most likely needed to establish the detailed reasons for the spectral observations.

Comparison of normal wavenumbers

It is worthwhile to compare the effects of successive OH substitution on the observed wavenumbers of flavone. However, a complete comparison of all modes for all the molecules examined here would be a lengthy and complex exercise. Instead, we will focus on a few regions of the spectrum, which might be of special interest. First, we should point out that the *O*–H stretching region would be of considerable interest, if it were observed experimentally. For 3-HF a line is predicted at 3420 cm^{-1} by DFT, while the 5-HF counterpart is indicated at 3566 cm^{-1}. In quercetin, there are five predicted wavenumbers between 3283 and 3675 cm^{-1}. All are predicted to have sufficient intensity to be observed in NR spectroscopy, but none are found. It is possible that molecule–molecule interactions in the solid either suppress or broaden these bands, making them invisible. They are not observed in our experiments in solution, or on Ag surfaces either.

Also of considerable interest are the most intense lines near 1600 cm^{-1}, which are usually termed the carbonyl-stretching region. In Fig. 13 we compare the normal FT-Raman spectra of flavone, 3-HF and 5-HF powder. The spectra of all the species consist of three or four intense lines and appear quite similar. However, the density functional calculation enables us to compare like vibrational modes, in a way not accessible just by observation of the spectrum. In Table 5 we summarize the observed wavenumbers, and their spectral assignments obtained from application of DFT. The lowest line in this region in each spectrum (1570, 1566, and 1569 cm^{-1}, respectively) may be assigned to the simultaneous Ring A, in-plane deformation, coupled to C═O stretch. Consequently, there is almost no shift of this line from flavone on OH substitution. However, the line at 1603 cm^{-1} in flavone is nearly unchanged in 5-HF, but drops slightly to 1594 cm^{-1} in the 3-hydroxy substituent. This vibration consists mainly of the Ring B quinoid-like C═C stretch, and is therefore also likely to have only a slight variation with substitution. The series starting at 1621 cm^{-1} in flavone is assigned to the in-plane deformation of all three rings (A, B and C), and is strongly influenced by substitution. Note the ν_{66} mode in 3-HF is not noticed in the spectrum, so we substitute the calculated (scaled) wavenumber in parentheses. The

DOI: 10.1002/jrs

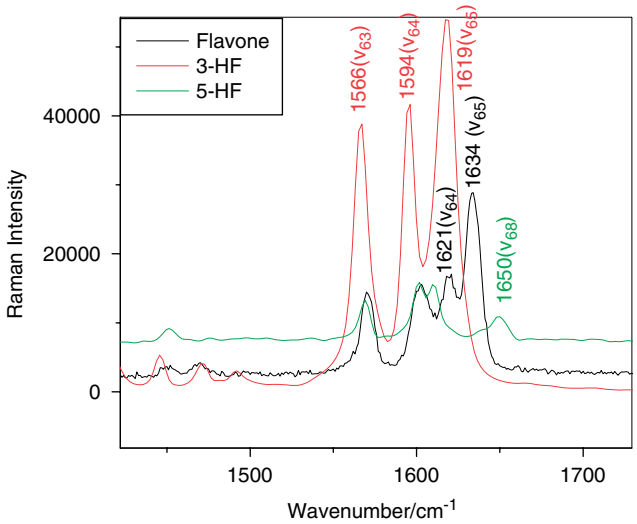

Figure 13. Comparison FT-Raman spectra in the C═O stretching region (1400–1800 cm^{-1}) of flavone, 3-hydroxyflavone and 5-hydroxyflavone powder. This figure is available in colour online at www.interscience.wiley.com/journal/jrs.

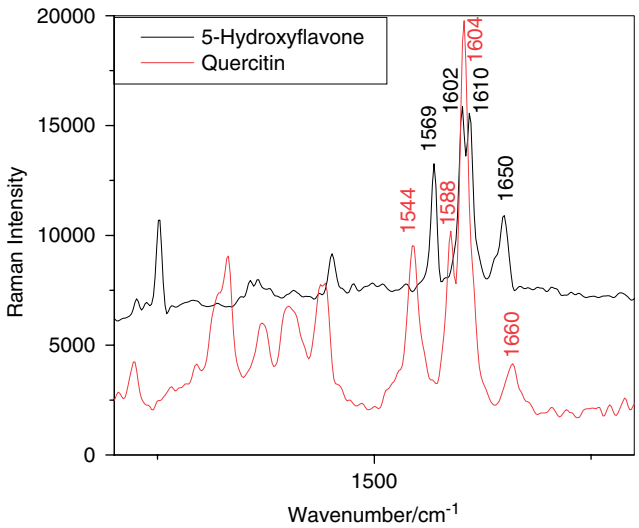

Figure 14. Comparison of the FT-Raman spectrum of solid 5-hydroxyflavone and quercitin in the region 1200–1800 cm^{-1}. This figure is available in colour online at www.interscience.wiley.com/journal/jrs.

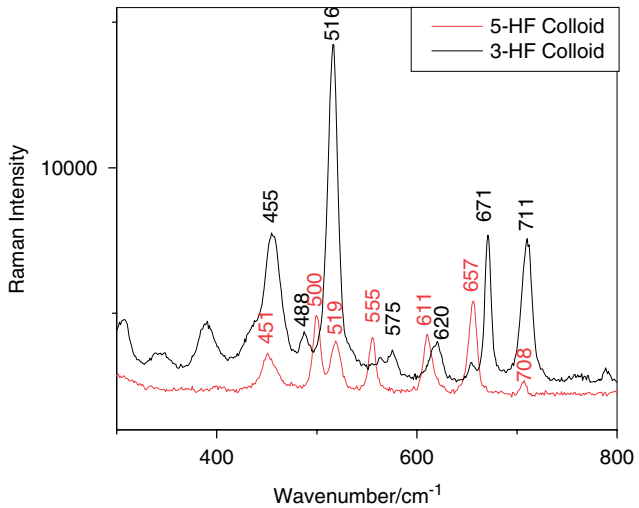

Figure 15. Modes of 3- and 5-hydroxy flavone, which are strongly enhanced on the colloid surface. The 200–800 cm^{-1} region is shown. This figure is available in colour online at www.interscience.wiley.com/journal/jrs.

most strongly perturbed line is the 1634 cm^{-1} flavone line attributed to C═O and C_2═C_3 stretching. This drops to 1619 cm^{-1} in 3-HF (below the ring deformation ν_{66}) but increases up to 1650 cm^{-1} in the 5-hydroxy derivative. The drop on 3-hydroxy substitution is caused by attachment of the —OH to the C_3 atom, which is an important part of the unperturbed vibration in flavone, while attachment of the —OH to the C_5 position has the opposite effect, adding a strong component of —OH bending to the normal mode. As mentioned in the previous section, all of these modes are considerably weakened in intensity on attachment to a silver surface, relative to several lower lying vibrations.

It is difficult to compare the spectrum of quercetin with all the other molecules owing to the fact that the normal modes of quercetin are dominated by the large number of OH bending modes. Despite this difficulty, the spectrum of quercetin resembles those of the other molecules. In Fig. 14, we show a comparison of the spectrum of quercetin with that of 5-HF in the region 1200–1800 cm^{-1}. This is the region that most closely resembles that of quercetin. From the strong resemblance we may infer that the modes ν_{75}, ν_{76}, ν_{78} and ν_{80} of quercetin may be associated with ν_{64}, ν_{66}, ν_{67} and ν_{68}, espectively, of 5-HF.

Several of the modes observed in 3- and 5-HF are quite strongly enhanced on the colloid or silver surface. In Fig. 15, we compare these modes, which appear in the region of 200–800 cm^{-1}. The observed increase in intensity of these modes converts them from some of the weakest bands in the solid to dominant bands on the colloid. The measured wavenumbers and assignments are listed in Table 6. It can be noticed that these lines are predominantly the ring C–C in-plane deformations. This indicates that the molecules are by and large (or at least have a large component) perpendicular to the metal surface. This is consistent with the simultaneous decrease in intensity of the higher frequency modes representing the C═O and C_2═C_3 stretch.

Persian berries – A case study

In order to demonstrate the potential of SERS as an ultrasensitive analytical tool in the identification of natural flavonoid dyes in works of art, we examined a microscopic sample from a modern silk fabric dyed using a Persian

berries extract in the Department of Textile Conservation at The Metropolitan Museum of Art. Persian berries is the name for a yellow dye obtained since antiquity from the dried unripe berries of plants in the buckthorn family (*Rhamnus*).[9] Our previous work on a variety of natural dyes[40,41] has shown that microscopic textile samples can be analyzed by SERS following a vapor phase treatment with hydrofluoric acid (HF) to hydrolyze the mordant dye complex. In this case, a 2 mm fragment of a silk thread from a modern textile dyed with Persian berries following traditional practice was treated for 15 min in a microchamber saturated with HF vapor. Following HF treatment, the sample was treated with a 2 µl drop of Ag colloid (diluted 20×) and 2 µl of a 0.2 M KNO_3 solution and the SERS spectrum measured directly from the microscopic colloidal aggregates deposited on the fiber.

The spectrum obtained from the microsample (Fig. 16) using 10 mW of 785 nm laser excitation clearly shows some of the quercetin bands, although the dye sample lines are somewhat broader and poorly resolved compared to our reference spectra. Note especially the prominent 1592 cm^{-1} band (ν_{76}) and the nearby shoulder at 1641 cm^{-1}. Furthermore, the intense line in the colloid spectrum of quercetin at 481 cm^{-1} shows up considerably weaker in the fabric microsample. The other bands present are probably due to other flavonoids such as rhamnetin and kaempferol, also contained in Persian berries.

It should be noted that although high-quality SERS spectra of the pure dyes have been obtained for all flavonoids, the current results show that further work on the treatment protocol for actual textile samples is needed in order to develop SERS into a routine technique for dye analysis. Nonetheless, the results shown here and the success we had with the same technique in the case of other natural dyes such as alizarin and berberine and some synthetic dyes[42] suggest that SERS has an enormous potential for analytical applications in which sampling is restricted to microscopic amounts.

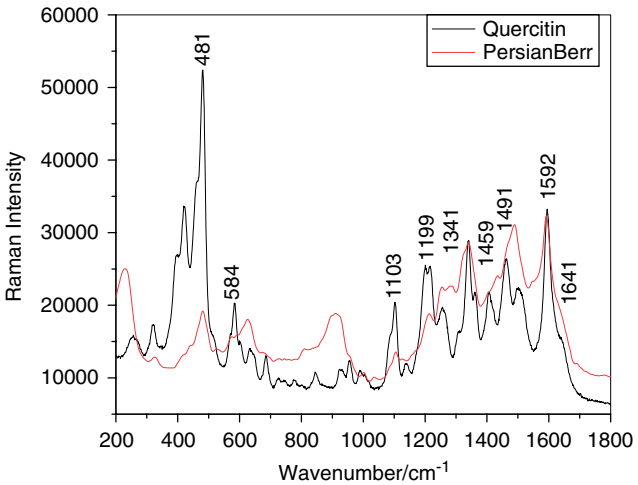

Figure 16. A comparison of the spectrum of quercitin on Ag colloid with that of the dye Persian berries, also on colloid. Spectra were obtained using 10 mW of the 785 nm excitation wavelength. This figure is available in colour online at www.interscience.wiley.com/journal/jrs.

CONCLUSIONS

We have obtained the Raman spectra of flavone and several hydroxy derivatives in powder form, as well as on Ag colloid, and where possible on Ag electrodes. The latter are enhanced by the technique of SERS, which enabled us to obtain intense spectra from a small quantity of material while simultaneously suppressing fluorescence. We have compared the relative intensities from the NR spectra with both colloidal and potential-dependent SERS and with DFT calculations. It is concluded that DFT calculations provide a source of accurate normal mode assignments, as well as a basis of comparison of the effects of successive OH substitutions on the normal modes of the parent flavone. A more detailed understanding of these environments should answer questions such as why the normal modes with C–*O*–H bending components are suppressed in the SERS spectra of the substituted flavones. Finally, we further provided a case study in the application of this technique to the identification of the active ingredient of a dye extracted from a textile.

Acknowledgements

We are indebted to the National Institute of Justice (Department of Justice Award #2006-DN-BX-K034) and the City University Collaborative Incentive program (#80209). This work was also supported by the National Science Foundation under Cooperative Agreement No. RII-9353488, grant No. CHE-0091362, CHE-0345987 and grant number ECS0217646 and by the City University of New York PSC-BHE Faculty Research Award Program. This research was also supported by the NIH/NIGMS/SCORE grant #GM08168 and an NCSA grant CHE050065 for computer facilities. Scientific research work at The Metropolitan Museum of Art was supported in part by grants from the Andrew W. Mellon Foundation, the David H. Koch Family Foundation, and the National Science Foundation Grant IMR 0526926 (which supplied the Bruker Senterra/Ramanscope combined Dispersive Raman/FT-Raman spectrometer). The Center for Analysis of Structures and Interfaces (CASI) provided support to Tatyana Teslova and Charlie Corredor from the Alfred P. Sloan Foundation.

REFERENCES

1. Harborne JB. *The Flavonoids: Advances in Research Since 1986*. Chapman and Hall: London, 1994.
2. Ferreira ESB, Hulme AN, McNab H, Quye A. *Chem. Soc. Rev.* 2004; **33**: 329.
3. Harborne JB, Marby TJ, Marby H. *The Flavonoids*. Chapman and Hall: London, 1975.
4. Harborne JB, Marby TJ. *The Flavonoids: Advances in Research*. Chapman and Hall: London, 1982.
5. McClure JW. In *Plant Flavonoids in Biology and Medicine: Biochemical, Pharmacological and Structure-Activity Relationships*,

Cody V, Middleton E, Harborne JB (eds). Alan R. Liss: New York, 1986; 77.
6. Geissman TA. *The Chemistry of Flavonoid Compounds*. The Macmillan Company: New York, 1962.
7. Smith DA, Banks SW. In *Plant Flavonoids in Biology and Medicine: Biochemical, Pharmacological and Structure-Activity Relationships*, Cody V, Middleton E, Harborne JB (eds). Alan R. Liss: New York, 1986; 113.
8. Gabor M. *The Pharmacology of Benzopyrone Derivatives and Related Compounds*. Akademiai Kiado: Budapest, 1986.
9. Hofenk de Graaff JH. *The Colorful Past. Origins, Chemistry and Identification of Natural Dyestuffs*. Abegg-Stiftung and Archetype Publications: Riggisberg, London, 2004.
10. Jose CI, Phadke PS, Rao AVR. *Spectrochem. Acta* 1974; **30A**: 1199.
11. Dean FM. *Naturally Occurring Oxygen Ring Compounds*. Butterworth: London, 1963; 280.
12. Marby TJ, Markham FK, Thomas MB. *The Systematic Identification of Flavonoids*. Springer: Berlin, 1970.
13. Sengupta PK, Kasha M. *Chem. Phys. Lett.* 1979; **68**: 382.
14. Brewer WE, Studet SL, Standiford M, Chou PT. *J. Phys. Chem.* 1989; **93**: 6088.
15. Dzugan TP, Schmidt J, Aartsma TJ. *Chem. Phys. Lett.* 1986; **127**(4): 336.
16. Looker JH, Hanneman WW. *J. Org. Chem.* 1962; **27**: 381.
17. Shaw L, Simpson TH. *J. Chem. Soc.* 1955; 655.
18. Hergert HL, Kurth EF. *J. Am. Chem. Soc.* 1953; **75**: 1622.
19. Looker JH, Hanneman WW, Kagal SA, Dappen JI, Edman JR. *J. Hetero-Cycl. Chem.* 1966; **3**: 55.
20. Looker JH, Kagal SA, Dappen JI, Edman JR. *J. Hetero-Cycl. Chem.* 1966; **3**: 61.
21. del Valle JC. *J. Chem. Phys.* 2006; **124**: 104506.
22. Briggs LH, Colebrook LD. *Spectrochim. Acta* 1962; **18**: 939.
23. Amaral DF, Arruda MSP, Arruda AC, Müller AH, Pantoja LLJ, da S, Lima TM. *J. Braz. Chem. Soc.* 2001; **12**(4): 538.
24. Torreggiani A, Trinchero A, Tamba M, Taddei P. *J. Raman Spectrosc.* 2005; **36**: 380.
25. Cornard JP, Merlin JC, Boudet AC, Vrielynck L. *Biospectroscopy* 1997; **3**(3): 183.
26. Petroski JM, Valente CDS, Kelson EP, Collins S. *J. Phys. Chem., A* 2002; **106**: 11714.
27. Livingstone RLG, Quagliano LG, Perez-Paz N, Munoz M, Tamargo MC, Jean-Mary F, Lombardi JR. SERS as sensing method for bio-molecules on MBE-grown quantum dots. In *Proceedings of SPIE.; Nanosensing: Materials and DevicesII*, Saif Islam M, Dutta AK (eds). SPIE-The International Society for Optical Engineering, Bellingham, WA, USA, 2005; 6008.
28. Daeid NN (ed.) Review Papers, 14th International Forensic Science Symposium, Interpol- Lyon, 19–22 October 2004 [Online]. Available: www.interpol.int/Public/Forensic/IFSS/meeting14/ReviewPapers.pdf.
29. Chen K, Leona M, Vo-Dinh KC, Yan F, Wabuyele MB, Vo-Dinh T. *J. Raman Spectrosc.* 2006; **37**: 520.
30. Birke RL, Lu T, Lombardi JR. *Techniques for Characterization of Electrodes and Electrochemical Processes*, Varma R, Selam JR (eds). John Wiley and Sons, Inc: New York, 1991; Chapt. 5.
31. Lee PC, Meisel D. *J. Phys. Chem.* 1982; **86**: 3391.
32. Frisch MJ, Trucks GW, Schlegel HB, Scuseria GE, Robb MA, Cheeseman JR, Montgomery JA Jr, Vreven T, Kudin KN, Burant JC, Millam JM, Iyengar SS, Tomasi J, Barone V, Mennucci B, Cossi M, Scalmani G, Rega N, Petersson GA, Nakatsuji H, Hada M, Ehara M, Toyota K, Fukuda R, Hasegawa J, Ishida M, Nakajima T, Honda Y, Kitao O, Nakai H, Klene M, Li X, Knox JE, Hratchian HP, Cross JB, Bakken V, Adamo C, Jaramillo J, Gomperts R, Stratmann RE, Yazyev O, Austin AJ, Cammi R, Pomelli C, Ochterski JW, Ayala PY, Morokuma K, Voth GA, Salvador P, Dannenberg JJ, Zakrzewski VG, Dapprich S, Daniels AD, Strain MC, Farkas O, Malick DK, Rabuck AD, Raghavachari K, Foresman JB, Ortiz JV, Cui Q, Baboul AG, Clifford S, Cioslowski J, Stefanov BB, Liu G, Liashenko A, Piskorz P, Komaromi I, Martin RL, Fox DJ, Keith T, Al-Laham MA, Peng CY, Nanayakkara A, Challacombe M, Gill PMW, Johnson B, Chen W, Wong MW, Gonzalez C, Pople JA. *Gaussian 03, Revision C.02*. Gaussian, Inc: Wallingford, CT, 2004.
33. Silman O, Bumm LA, Callaghan R, Blatchford CG, Kerker M. *J. Phys. Chem.* 1983; **87**: 1014.
34. Wang M, Teslova T, Xu F, Lombardi JR, Birke RL, Leona M. *J. Phys. Chem.* 2007; DOI: 10.1021/jp062100i.
35. Wang M, Spataru T, Lombardi JR, Birke RL. *J. Phys. Chem.* 2007; DOI: 10.1021/jp0650937.
36. Rauhut G, Pulay P. *J. Phys. Chem.* 1995; **99**: 3093.
37. Pulay P, Fogarasi G, Pongor G, Boggs JE, Vargha A. *J. Am. Chem. Soc.* 1983; **105**: 7037.
38. Neugebauer J, Hess BA. *J. Chem. Phys.* 2003; **118**: 7215.
39. Sanchez-Cortes S, Francioso O, Garcia-Ramos JV, Ciavatta C, Gessa C. *Colloids Surf. A: Physicochem. Eng. Aspects* 2001; **176**: 177.
40. Leona M, Stenger J, Ferloni E. *J. Raman Spectrosc.* 2006; **37**: 981.
41. Leona M. Surface enhanced Raman scattering in art and archaeology, Proc. of SPIE Vol. 5993, 5993L-1. SPIE-The International Society for Optical Engineering, Bellingham, WA, USA, 2005.
42. Leona M. *Identification of Natural Dyes in Works of art by SERS Techniques: Recent Progress and Remaining Problems*. ICORS: Yokohama, 2006;; 20, August 2006.